AD-A279 163

|||||||||||||||||||||||||||||||||||||

DOT/FAA/CT-93/68

FAA Technical Center
Atlantic City International Airport,
N.J. 08405

Stress-Intensity Factor Solutions for Cracks at Countersunk Rivet Holes Under Uniaxial Tension
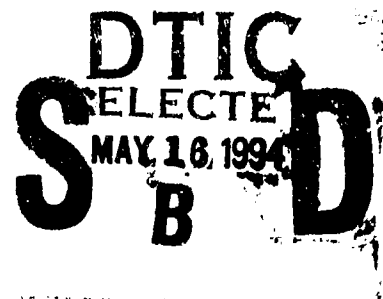
February 1994

Final Report

This document is available to the public
through the National Technical Information
Service, Springfield, Virginia 22161.

DTIC
SELECTE
MAY 16, 1994
S
B
D

Ⓞ
U.S. Department of Transportation
Federal Aviation Administration

94-14396
||||||||||||||||||||||||||||||

DTIC QUALITY INSPECTED 1

94   5   13   032

NOTICE

This document is disseminated under the sponsorship of the U. S. Department of Transportation in the interest of information exchange. The United States Government assumes no liability for the contents or use thereof.

The United States Government does not endorse products or manufacturers. Trade or manufacturers' names appear herein solely because they are considered essential to the objective of this report.

1. Report No.	2. Government Accession No.	3. Recipient's Catalog No.
DOT/FAA/CT-93/68		

4. Title and Subtitle		5. Report Date
STRESS-INTENSITY FACTOR SOLUTIONS FOR CRACKS AT COUNTERSUNK RIVET HOLES UNDER UNIAXIAL TENSION		February 1994
		6. Performing Organization Code
		ACD-220

7. Author's)	8. Performing Organization Report No.
P.W. Tan*, C.A. Bigelow`, P.E. O'Donoghue+, and S.N. Atluri#	

9. Performing Organization Name and Address	10. Work Unit No. (TRAIS)
Federal Aviation Administration Technical Center Atlantic City International Airport, NJ 08405	11. Contract or Grant No.
	13. Type of Report and Period Covered

12. Sponsoring Agency Name and Address	13. Type of Report and Period Covered
U.S. Department of Transportation Federal Aviation Administration Technical Center Atlantic City International Airport, NJ 08405	Final Report
	14. Sponsoring Agency Code

15. Supplementary Notes

*FAA Technical Center, Atlantic City International Airport New Jersey
`Mail Stop 188E, NASA Langley Research Center, Hampton, Virginia
+Dept. of Civil Engineering, University College, Dublin, Ireland
#FAA Center of Excellence, Georgia Institute of Technology, Atlanta, GA

16. Abstract

To predict crack growth and fracture strengths of riveted joints subjected to widespread fatigue damage, accurate stress and fracture analyses of corner and surface cracks at a rivet hole are needed. The results presented in this report focus on the computation of stress-intensity factor solutions for rivet holes with cracks. The stress-intensity factor solutions for surface and corner cracks at countersunk rivet holes in a plate were obtained using the finite-element-alternating technique. A range of crack shapes, crack sizes, and crack locations under remote tension were considered.

17. Key Words	18. Distribution Statement
Boundary Correction Factors Surface Cracks Corner Cracks Finite-Element-Alternating Method	Document is available to the public through the National Technical Information Service, Springfield, Virginia 22161

19. Security Classif. (of this report)	20. Security Classif. (of this page)	21. No. of Pages	22. Price
Unclassified	Unclassified	30	

Form DOT F 1700.7 (8-72)   Reproduction of completed page authorized

Table of Contents

iii

LIST OF ILLUSTRATIONS

LIST OF TABLES

EXECUTIVE SUMMARY

To predict crack growth and fracture strengths of riveted joints subjected to widespread fatigue damage, accurate stress and fracture analyses of corner and surface cracks at a rivet hole are needed. The results presented in this report focus on the computation of stress-intensity factor solutions for rivet holes with cracks. The stress-intensity factor solutions for surface and corner cracks at countersunk-rivet holes in a plate were obtained using the finite-element-alternating technique. A range of crack shapes and crack sizes under remote tension were analyzed. Three crack locations were considered: the upper edge of the countersunk bore (designated as crack location 1), the knee between the countersunk and straight shank portion (crack location 2), and the lower edge of the straight shank hole (crack location 3).

For cracks at location 1, cracks with shapes nearer to a semicircle ($a/c = 0.7$) generally gave higher boundary correction factors because more of the crack front is closer to the free surface. However, as the crack becomes deeper, more of the crack front lies further from the surface; hence, the crack front was in a region of more uniform stresses. The boundary correction factors were also highest at locations where the crack front approached the countersunk surface of the rivet hole.

For cracks at location 2, the highest values of the boundary correction factors were found at the free surfaces for $a/c = 0.4$ and $a/t = 0.4$. This same crack configuration also produced the smallest values of boundary correction factors, calculated at the deepest point on the crack profile, for crack location 2. Again, the boundary correction factors were highest at locations where the crack front approached the countersunk surface of the rivet hole.

For cracks at location 3, cracks with shapes nearer to a semicircle ($a/c = 0.7$) generally gave higher boundary correction factor because more of the crack front is closer to the free surface. However, as the crack becomes deeper, more of the crack front lies further from the surface; hence, the crack front was in a region of more uniform stresses. The boundary correction factors were highest at locations where the crack front approached the interior surface of the straight shank of the rivet hole.

INTRODUCTION

Aging aircraft research activities being conducted worldwide are aimed at developing and implementing advanced fatigue and fracture mechanics concepts into the damage tolerance analysis methodology for the aging, current, and next generation fleets. These activities include the development and implementation of a damage tolerance analysis methodology for widespread fatigue damage (WFD).

From in-service experience reports by aircraft fleet operators, the riveted lap splice joints of their aging fleet have been identified as one of the critical locations on an aircraft that is susceptible to WFD. Widespread fatigue damage at riveted lap splice joints is usually in the form of multiple cracks emanating from the stress concentrations in the rivet holes. Thus, one of the objectives of the Federal Aviation Administration's Aging Aircraft Research Program on WFD is to develop the methodology to predict crack initiation, crack growth rates, and residual strengths of aircraft structures subjected to WFD.

To reliably predict crack growth rates and fracture strengths of riveted joints subjected to WFD, accurate stress and fracture analyses of corner and surface cracks at a rivet hole are needed. Therefore, the results presented in this paper focus on the computation of the stress-intensity factor solutions for rivet holes with cracks.

Many stress analyses of three-dimensional crack configurations have been done in the last two decades (references 1 to 19). Various methods have been used to obtain stress-intensity factors for surface and corner cracks in plates: the alternating method (1, 2, 7), the finite-element method with singularity elements (3, 4, 10, 13, 19), the finite-element method with displacement hybrid elements (5, 6), the finite-element-alternating method (14, 15, 18), and the boundary-integral equation method (9). Stress-intensity factor equations have also been obtained by fitting empirical equations to some of the stress-intensity factors obtained by finite-element analyses (11, 16, 17).

Surface and corner cracks at holes have also been considered by many investigators. Smith and Kulgren (8) and Raju and Newman (12) analyzed a corner crack at a circular hole using the alternating method and the finite-element method, respectively. Nishioka and Atluri (15, 18) analyzed a corner crack at a circular hole and in a lug using the finite-element-alternating method. The stress-intensity factors obtained by all of the above mentioned methods agreed well with one another (12, 15) except in the region where the crack intersected the hole boundary.

In an AGARD Short-Crack Cooperative Test Program (20), the stress-intensity factor solution used for small surface and corner cracks emanating from an edge notch was based on previous solutions for cracks at holes (16), the notch stress-concentration factor, and engineering judgment. In an effort to establish a more accurate solution, a cooperative program between the National Aeronautical and Space Administration (NASA) and the Chinese Aeronautical Establishment (CAE) (21) used two different methods to obtain stress-intensity factor solutions. Zhao and Wu (22, 23) used the three-dimensional weight-function method; Tan et al. (24) and Shivakumar and Newman (25) used the three-dimensional finite-

element method. Tan, et al., used three-dimensional finite-element analyses to obtain stress-intensity factor solutions for a wide range of corner cracks at the semicircular edge notch in a finite thickness plate subjected to remote tensile loading. However, no solutions exist for corner and surface cracks at countersunk rivet holes. The purpose of this report is to present results for cracks in countersunk rivet holes.

The stress-intensity factor solutions for surface and corner cracks at countersunk rivet holes in a plate were obtained using the three-dimensional finite-element-alternating technique. A range of crack shapes, sizes, and locations were considered.

In the following sections, the finite-element-alternating method (FEAM) is briefly described. The configurations analyzed and the finite-element models used are presented. Stress-intensity factor solutions for the cases analyzed are presented and discussed.

FINITE-ELEMENT-ALTERNATING METHOD

The Schwartz-Neumann alternating method is used to obtain the stress-intensity factor solutions for a crack in a finite body. References 28 and 29 provide a more detailed description of this procedure. In the alternating method as applied to a crack in a finite solid, two types of solutions are required. First, a general analytical solution for an embedded elliptical crack in an infinite body subjected to arbitrary crack face tractions is required. A potential function approach is adopted based on the well-known Trefftz formulation (30). The work of Nishioka and Atluri (28) presents further details on this technique. Second, a numerical scheme (in this case, the finite-element method) is needed to solve for the stresses in the uncracked finite body.

In the finite-element-alternating method, the finite-element method is used to analyze the uncracked finite body under the given external loads. The geometry of the uncracked body is identical to that of the cracked body except for the crack itself. Since the crack is not explicitly modeled, nonzero stresses are calculated at the location of the actual crack. These fictitious stresses must be removed in order to create the traction-free crack surface existing in the actual problem. The analytical solution for an infinite body with an embedded elliptical crack is known for an arbitrary distribution of tractions on the crack face. To create the stress-free crack face, a polynomial function for the inverse of these fictitious stresses is determined using a least square fit and applied to the infinite cracked body. The stresses on the external surfaces of the finite body due to the applied loads on the crack faces are calculated. The inverse of these stresses is applied as an external load on the finite uncracked body. This addition to the external loads again creates fictitious stresses at the crack location which must be removed to obtain the stress-free crack faces in the actual configuration. All steps in the iteration are repeated until the stresses on the crack surface become negligible. For the cases presented here, this iteration process took from three to eight steps depending on the configuration. The overall stress-intensity factor solution is obtained by adding the stress-intensity factor solutions for all the iterations.

To analyze the uncracked body, the three-dimensional finite-element method with 20-noded isoparametric elements was used. It is necessary that the finite-element mesh used to

2

describe the uncracked body be refined enough to accurately characterize the stress distribution in the uncracked body. If the geometry and applied loading of the configuration are relatively simple, not as many elements are required since the stress state is not complex. However, if either the geometry or the loading is such that there are significant stress gradients in the uncracked body, then a greater number of elements will be required. It is also necessary that there be enough refinement in the region of the crack to accurately fit a polynomial distribution to the fictitious stresses on the crack face. For the configurations analyzed here, it was found that a minimum of two elements along the major and minor axes of the crack face were required.

CONFIGURATIONS AND LOADING

The loading considered in the present work is a remote uniform tension (S= 1.0 MPa), as shown in figure 1. Figure 2 shows the general configuration of the countersunk hole that was analyzed. The half-height of the plate (H) and width (W) were chosen to be large enough to have a negligible effect on the stress-intensity factors (H/W = 2) and the ratio of the maximum hole radius to plate width (W/R_1) was selected as 5. The radius of the straight shank hole is defined to be R. Three crack locations were considered with a range of crack depth to plate thickness (a/t) of 0.2, 0.3, and 0.4, and crack depth to crack length (a/c) of 0.4, 0.7 and 2.0. For all crack locations, the ratio of the length of the straight shank portion of the hole to the plate thickness (h/t) was set equal to 0.5. For all calculations, the total angle subtended by the countersunk hole was set to 100°.

STRESS-INTENSITY FACTOR

The remote tensile loads cause only mode I deformations. The mode I stress-intensity factor (K) at any location along the crack front was expressed as

$$K = S (\pi a/Q)^{1/2} F (a/t, a/c, h/t, R/t, \phi)$$

Values of F, the boundary-correction factor, were calculated along the crack front for various combinations of parameters (a/t, a/c, and ϕ). The crack dimensions and angle ϕ are defined in figure 2. Note that the angle ϕ is not the standard definition of a parametric angle (the angle measured with reference to the circle contained within the ellipse) but is instead the physical angle as shown in figure 2 and is measured differently at each crack location. The shape factor for an ellipse, Q, is given by the square of the complete elliptic integral of the second kind. Empirical expressions for Q (9) are

$$Q = 1 + 1.464 (a/c)^{1.65} \qquad \text{for a/c} \leq 1$$

$$Q = 1 + 1.464 (c/a)^{1.65} \qquad \text{for a/c} > 1$$

Convergence studies were done to determine the needed mesh refinement. Typical results for the convergence study at crack location 3, with a/t = 0.2 and a/c = 0.4, are shown in figure 3. Results are presented in terms of F, the boundary correction factor. Convergence was obtained very quickly, and the mesh with 372 elements was used for the remainder of the calculations at location 3. Table 1 shows the number of elements, nodes, degrees of freedom

(DOF), and the computer processing units (CPU) seconds required to execute the program on a DECStation 5000/200 for each crack location. As shown in table 1, a more refined mesh was required at location 2 compared to locations 1 and 3. Figure 4(a) shows a plan view of the mesh that was used for crack location 2; figure 4(b) shows an enlarged view of the mesh near the crack location.

RESULTS AND DISCUSSION

The boundary correction factors (F) obtained with the FEAM analyses are presented in tables 2, 3, and 4 for crack locations 1, 2, and 3, respectively.

Figures 5, 6, and 7 present the variation in the boundary correction factor (F) along the crack for crack location 1 for a/c = 0.4, 0.7, and 2.0, respectively. Each figure shows the variation in F for the three values of a/t = 0.2, 0.3, and 0.4. Inserts in the figures show the crack shapes and the angle definition. The three figures show distinctly different behaviors for the three a/c ratios. For a/t = 0.3 and 0.4, the maximum values of F are found at $\phi_1 = 140^o$ where the crack profile intersects the countersunk surface of the rivet hole. For a/t = 0.2, the maximum values of F is found at $\phi_1 = 110^o$ near to but not at the intersection of the crack front and the countersunk surface of the rivet hole. The largest value of F is calculated for a/c = 0.7. There is not much difference between the three curves for F for the different a/t ratios.

Figures 8, 9, and 10 present the variation in the boundary correction factor (F) along the crack for crack location 2 for a/c = 0.4, 0.7, and 2.0, respectively. Each figure shows the variation in F for the three values of a/t = 0.2, 0.3, and 0.4. Inserts in the figures show the crack shapes and the angle definition. The three figures show distinctly different behaviors for the three a/c ratios. For a/c = 0.4 and 0.7, the maximum values of F are found at $\phi_2 = 130^o$ where the crack profile intersects the countersunk surface of the rivet hole. For a/c = 2.0, the maximum value of F is near $\phi_2 = 85^o$. The largest value of F is calculated for a/c = 0.4 and a/t = 0.4. Again, there is not much difference between the three curves for F for the different a/t ratios.

Figures 11, 12, and 13 present the variation in the boundary correction factor (F) along the crack for crack location 3 for a/c = 0.4, 0.7, and 2.0, respectively. Each figure shows the variation in F for the three values of a/t = 0.2, 0.3, and 0.4. Inserts in the figures show the crack shapes and the angle definition. The three figures again show distinctly different behaviors for the three a/c ratios. For a/c = 0.4 and 0.7, the maximum values of F are found at $\phi_3 = 90^o$ where the crack profile intersects the interior surface of the straight shank portion of the rivet hole. For a/c = 2.0, the maximum value of F is near $\phi_3 = 0^o$ where the crack profile intersects the bottom face of the plate. The largest value of F is calculated for a/c = 0.7 and a/t = 0.4. Again, there is not much difference between the three curves for F for the different a/t ratios.

CONCLUDING REMARKS

The stress-intensity factor solutions for surface and corner cracks at countersunk-rivet holes in a plate were obtained using the finite-element-alternating technique. A range of crack shapes and crack sizes under remote tension were analyzed. Three crack locations were considered: the upper edge of the countersunk bore (designated as crack location 1), the knee between the countersunk and straight shank portion (crack location 2), and the lower edge of the straight shank hole (crack location 3).

For cracks at location 1, cracks with shapes nearer to a semicircle ($a/c = 0.7$) generally gave higher boundary correction factors because more of the crack front is closer to the free surface. However, as the crack becomes deeper, more of the crack front lies further from the surface; hence, more of the crack front is in a region of lower stress gradient. For all crack shapes, the boundary correction factors were highest at locations where the crack front approached the countersunk surface of the rivet hole, where the larger stress gradients are expected.

For cracks at location 2, the highest values of the boundary correction factors were found at the points where the crack fronts intersect the free surfaces for the case of $a/c = 0.4$ and $a/t = 0.4$. This combination of a/t and a/c produced an elongated, sharper crack shape which resulted in larger stress gradients, compared to other crack configurations. This same crack configuration also produced the smallest values of boundary correction factors, calculated at the deepest point on the crack profile, for crack location 2. This is again due to the elongated shape of the crack, where now the crack tip at the deepest point is relatively distant from the boundaries, thus, in a region of lower stress gradient.

For cracks at location 3, cracks with shapes nearer to a semicircle ($a/c = 0.7$) generally gave higher boundary correction factors because more of the crack front is closer to the free surface where larger stress gradients are expected. As the crack becomes deeper and more of the crack front lies further from the surface, the boundary correction factors decrease since the crack front is in a region of lower stress gradient. The boundary correction factors were highest at locations where the crack front approached the interior surface of the straight shank of the rivet hole.

REFERENCES

(1)   Shah, R. C., and Kobayashi, A. S., On the Surface Flaw Problem. *Surface Crack: Physical Problems and Computational Solutions*. J. L. Swedlow (Ed.), ASME, American Society of Mechanical Engineers, 1972, pp. 79-142.

(2)   Smith, F. W., The Elastic Analysis of the Part-Circular Surface Flaw Problem by the Alternating Method. *Surface Crack: Physical Problems and Computational Solutions*, J. L. Swedlow (Ed.), ASME, American Society of Mechanical Engineers, 1972, pp. 125-152.

(3)   Tracey, D. M.,. 3D Elastic Singularity Element for Evaluation of K Along an Arbitrary Crack Front. *Int. J. of Fracture*, Vol. 9, 1973, pp. 340-343.

(4)   Tracey, D. M., Finite Element for Three-Dimensional Elastic Crack Analysis. *Nuclear Engineering and Design*, Vol. 26, 1974.

(5)   Atluri, S. N., and Kathiresan, K., An Assumed Displacement Hybrid Finite Element Model for Three-Dimensional Linear Elastic Fracture Mechanics Analysis. *Proceedings of the 12th Annual Meeting of the Soc. Engr. Science*, University of Texas, Austin, 1975.

(6)   Kathiresan, K., Three-Dimensional Linear Elastic Fracture Mechanics Analysis by a Displacement Hybrid Finite Element Model. Ph. D. Thesis, Georgia Institute of Technology, 1976.

(7)   Kobayashi, A. S., and Enetanya, A. N., Stress Intensity Factor of a Corner Crack. *Mechanics of Crack Growth, ASTM STP 590*, American Society for Testing and Materials, 1976, pp. 477-495.

(8)   Smith, F. W., and Kulgren, T. E., Theoretical and Experimental Analysis of Surface Cracks Emanating From Fastener Holes. AFFDL-TR-76-104, Air Force Flight Dynamics Laboratory, 1977.

(9)   Raju, I. S., and Newman, J. C., Jr., Stress-Intensity Factors for a Wide Range of Semi-Elliptical Surface Cracks in Finite-Thickness Plates. *Engineering Fracture Mechanics*, Vol. 11, No. 4, 1979, pp. 817-829.

(10)   Newman, J. C., Jr. and Raju, I. S., Analyses of Surface Cracks in Finite Plates Under Tension and Bending Loads. NASA TP-1578, 1979.

(11)   Heliot, J., Labbens, R. C., and Pellissier-Tanon, A., Semi-Elliptical Surface Cracks Subjected to Stress Gradients. *Fracture Mechanics, ASTM STP 677*, C.W. Smith (Ed.), American Society for Testing and Materials, 1979, pp. 341-364.

(12) Raju, I. S., and Newman, J. C., Jr., Stress-Intensity Factors for Two Symmetric Corner Cracks. *Fracture Mechanics, ASTM STP 677*, C. W. Smith (Ed.), American Society for Testing and Materials, 1979, pp. 411-430.

(13) Pickard, A. C. Stress-Intensity Factors for Cracks with Circular and Elliptic Crack Fronts - Determined by 3D Finite Element Methods. PNR-90035, Rolls Royce Limited, May 1980.

(14) Nishioka, T., and Atluri, S. N., Analytical Solution for Embedded Elliptical Cracks, and Finite Element-Alternating Method for Elliptical Surface Cracks, Subjected to Arbitrary Loadings. *Engineering Fracture Mechanics*, Vol. 17, 1983, pp. 247-268.

(15) Nishioka, T., and Atluri, S. N., An Alternating Method for Analysis of Surface Flawed Aircraft Structural Components. *AIAA Jnl.*, Vol. 21, 1983, pp. 749-757.

(16) Newman, J. C., Jr., and Raju, I. S., Stress-Intensity Factor Equations for Cracks in Three-Dimensional Finite Bodies. *Fracture Mechanics: Fourteenth Symposium - Volume I: Theory and Analysis. ASTM STP 791*, J. C. Lewis and G. Sines (Eds.), American Society for Testing and Materials, 1983, pp. I238-I265.

(17) Newman, J. C., Jr., and Raju, I. S., Stress-Intensity Factor Equations for Cracks in Three-Dimensional Finite Bodies Subjected to Tension and Bending Loads. NASA TM-85793, April 1984.

(18) Atluri, S. N., and Nishioka, T., Computational Methods for Three-Dimensional Problems of Fracture. *Computational Methods in Mechanics of Fracture*, S. N. Atluri (Ed.), North Holland, Chapter 7, 1986, pp. 230-287.

(19) Raju, I. S. and Newman, J. C., Jr., Stress-Intensity Factors for Corner Cracks in Rectangular Bars. *Fracture Mechanics: Nineteenth Symposium, ASTM STP 969*, T. A. Cruse (Ed.), American Society for Testing and Materials, 1988, pp. 43-55.

(20) Newman, J. C., Jr. and Edwards, P. R., Short-Crack Growth Behavior in an Aluminum Alloy - An AGARD Cooperative Test Programme, AGARD R-732, 1988.

(21) Newman, J. C. Jr., Wu, X. R., Venneri, S. L. and Li, C. G., Small-Crack Effects in High-Strength Aluminum Alloys - A NASA/CAE Cooperative Program, NASA RP-1309, 1993.

(22) Zhao, W. and Wu, X. R., Stress-Intensity Factor Evaluation by Weight Function for Surface Crack in Edge Notch. *Theoretical and Applied Fracture Mechanics*, Vol. 13, 1990, pp. 225-238.

(23) Zhao, W. and Wu, X. R., Stress-Intensity Factors for Corner Cracks at a Semi-Circular Notch Under Stress Gradients. *Fatigue and Fracture of Engineering Materials and Structures*, Vol. 13, No. 4, 1990, pp. 347-360.

(24)   Tan, P. W., Raju, I. S., Shivakumar, K. N., and Newman, J. C., Jr., Evaluation of Finite-Element Models and Stress-Intensity Factors for Surface Cracks Emanating from Stress Concentrations. *Surface-Crack Growth: Models, Experiments and Structures, ASTM STP 1060*, W. G. Reuter, J. H. Underwood and J. C. Newman, Jr. (Eds.), American Society for Testing and Materials, 1990, pp. 34-48.

(25)   Shivakumar, K. N. and Newman, J. C., Jr., Stress-Intensity Factors for Large Aspect Ratio Surface and Corner Cracks at a Semi-Circular Notch in a Tension Specimen. *Engineering Fracture Mechanics*, Vol. 38, No. 6, 1991, pp. 467-473.

(26)   Newman, J. C., Jr.: Fracture Mechanics Parameters for Small Fatigue Cracks. *Small-Crack Test Methods, ASTM STP 1149*, American Society for Testing and Materials, 1992, pp. 6-28.

(27)   Tan, P. W., Newman, J. C., Jr., and Bigelow, C. A., Three-Dimensional Finite-Element Analyses of Corner Cracks at Stress Concentrations. Durability of Metal Aircraft, Proceedings of the International Workshop on Structural Integrity of Aging Airplanes, Atlanta, GA, March 31- April 2, 1992, S. N. Atluri, C. E. Harris, A. Hoggard, N. Miller, and S. G. Sampath, (Eds.), Atlanta Technology Publications, Atlanta, GA, pp. 167-186.

(28)   Nisioka, T. and Atluri, S. N., Analytical Solutions for Embedded Elliptical Cracks and Finite Element Alternating Method for Elliptical Cracks Subjected to Arbitrary Loading. *Engineering Fracture Mechanics*, Vol. 17, 1983, pp. 247-268.

(29)   Sih, G. C. and Liebowitz, H., Mathematical Theories of Brittle Fracture, Fracture, An Advanced Treatise, Vol. II, H. Leibowitz, (Ed.), Academic Press, New York, 1968, pp. 68-188.

(30)   Trefftz, E., Handbuch der Physik, Vol. 6, p. 92, Springer Verlag, Berlin, 1928.

Table 1.   Statistics for FEAM meshes

Crack Location	DOF	No. Elements	No. Nodes	CPU Seconds
1	6141	372	2145	4260
2	7965	496	2655	9150
3	6141	372	2145	4260

Table 2. Boundary-correction factors F for a corner crack (location 1) at a countersunk rivet hole in a plate under tension (R/t = 2.0, h/t = 0.5; F = $K/(S(\pi a/Q)^{1/2})$)

ϕ_1 (degrees)	F a/c = 0.4		
	a/t = 0.2	a/t = 0.3	a/t = 0.4
0	1.4553	1.4856	1.5513
3.319	1.4872	1.5176	1.5739
6.756	1.5859	1.61	1.6549
10.447	1.7223	1.7486	1.7883
14.56	1.8717	1.8967	1.9258
19.328	2.0241	2.0389	2.054
25.091	2.1736	2.1728	2.172
32.367	2.3157	2.2995	2.2839
41.927	2.4478	2.4156	2.3926
54.799	2.561	2.5175	2.4952
71.761	2.648	2.5969	2.5845
91.849	2.7032	2.6466	2.6522
111.58	2.7235	2.6632	2.6901
127.8	2.7075	2.6455	2.6942
140	2.664	2.604	2.6686
ϕ_1 (degrees)	F a/c = 0.7		
	a/t = 0.2	a/t = 0.3	a/t = 0.4
0	2.2625	2.2883	2.3913
6.521	2.254	2.2634	2.2484
13.217	2.2795	2.2717	2.2364
20.275	2.3338	2.3105	2.2556
27.894	2.4051	2.3646	2.2916
36.29	2.485	2.4298	2.3385
45.68	2.5716	2.5047	2.3973
56.231	2.6616	2.5893	2.467
67.978	2.7483	2.6766	2.5486
80.707	2.8281	2.764	2.6399
93.911	2.8926	2.8417	2.7372
106.91	2.9419	2.9055	2.8345
119.1	2.9725	2.954	2.9234
130.15	2.9911	2.9928	2.999
140	3.0013	3.0275	3.0591

Table 2. continued $(R/t = 2.0, h/t = 0.5; F = K/(S(\pi a/Q)^{1/2}))$

ϕ_1 (degrees)	F a/c = 2.0		
	a/t = 0.2	a/t = 0.3	a/t = 0.4
0	1.9677	2.0744	2.1281
21.66	1.9066	1.9834	2.018
39.558	1.8165	1.8649	1.8808
53.134	1.708	1.7351	1.7338
63.375	1.595	1.6054	1.5902
71.466	1.4758	1.4757	1.4519
78.236	1.3643	1.3572	1.3298
84.253	1.2833	1.2748	1.2477
89.926	1.2604	1.2536	1.2283
95.594	1.3093	1.3073	1.2877
101.6	1.4208	1.4295	1.4184
108.34	1.5659	1.5954	1.5966
116.39	1.7157	1.7788	1.8019
126.56	1.8929	2.0008	2.0558
140	2.258	2.4125	2.5052

Table 3.   Boundary-correction factors F for a surface crack (location 2) at a countersunk rivet hole in a plate under tension ($R/t = 2.0$, $h/t = 0.5$; $F = K/(S(\pi a/Q)^{1/2})$)

ϕ_2 (degrees)	F a/c = 0.4		
	a/t = 0.2	a/t = 0.3	a/t = 0.4
0	3.7943	3.7105	3.9439
25.994	3.5563	3.4155	3.5715
45.392	3.256	3.0684	3.1077
58.476	2.9193	2.6964	2.605
67.604	2.5769	2.3303	2.1289
74.454	2.2519	1.9927	1.736
80.004	1.9617	1.7072	1.4497
84.831	1.7397	1.5022	1.2733
89.317	1.6483	1.4311	1.222
93.76	1.747	1.5472	1.2312
98.446	2.0197	1.8446	1.6221
103.72	2.4086	2.2865	2.0992
110.09	2.8773	2.8528	2.7958
118.37	3.3967	3.5139	3.6884
130	3.9234	4.2093	4.6621
ϕ_2 (degrees)	F a/c = 0.7		
	a/t = 0.2	a/t = 0.3	a/t = 0.4
0	3.7878	3.7667	3.8073
14.155	3.6672	3.592	3.5864
27.502	3.5228	3.3687	3.3305
39.555	3.3614	3.1232	3.0531
50.211	3.1984	2.8916	2.7792
59.623	3.0438	2.6933	2.5378
68.051	2.913	2.5435	2.3541
75.767	2.8179	2.4506	2.246
83.03	2.7737	2.4256	2.2268
90.074	2.7924	2.4742	2.3012
97.12	2.8739	2.6073	2.4766
104.39	3.0166	2.825	2.7504
112.12	3.2052	3.1204	3.1215
120.56	3.4226	3.4658	3.5719
130	3.6502	3.8042	4.0572

12

Table 3. continued $(R/t = 2.0, h/t = 0.5; F = K/(S(\pi a/Q)^{1/2}))$

ϕ_2 (degrees)	F a/c = 2.0		
	a/t = 0.2	a/t = 0.3	a/t = 0.4
0	1.7661	1.7563	1.7846
4.047	1.7829	1.7688	1.7879
8.217	1.8501	1.8299	1.8375
12.643	1.9479	1.9222	1.9196
17.488	2.0624	2.032	2.0147
22.958	2.1801	2.148	2.1109
29.323	2.2931	2.2615	2.2038
36.943	2.3924	2.3638	2.2869
46.266	2.4734	2.4486	2.3572
57.747	2.5315	2.511	2.4123
71.575	2.5651	2.5484	2.4479
87.197	2.5773	2.5597	2.4652
103.13	2.5666	2.5484	2.463
117.7	2.5376	2.5185	2.4436
130	2.4933	2.4748	2.4123

Table 4.   Boundary-correction factors F for a surface crack (location 3) at a countersunk rivet hole in a plate under tension (R/t = 2.0, h/t = 0.5; F = $K/(S(\pi a/Q)^{1/2})$)

ϕ_3 (degrees)	F a/c = 0.4		
	a/t = 0.2	a/t = 0.3	a/t = 0.4
0	1.5961	1.5911	1.6293
4.034	1.6628	1.6361	1.6508
8.283	1.8413	1.7948	1.7873
13.004	2.0792	2.0187	1.9904
18.554	2.3433	2.2758	2.2346
25.487	2.6132	2.5507	2.5075
34.715	2.8744	2.8232	2.7917
47.7	3.1065	3.0731	3.0626
66.211	3.2922	3.3135	3.2955
90	3.4199	3.4333	3.4709
ϕ_3 (degrees)	F a/c = 0.7		
	a/t = 0.2	a/t = 0.3	a/t = 0.4
0	2.5122	2.3535	2.3769
7.036	2.5325	2.3549	2.3469
14.294	2.6073	2.4173	2.3865
22.006	2.7228	2.5296	2.4874
30.429	2.8604	2.6822	2.6399
39.836	3.0098	2.8639	2.8273
50.485	3.1593	3.058	3.0267
62.527	3.2969	3.2453	3.2164
75.862	3.4124	3.4034	3.3774
90	3.499	3.5212	3.4999

Table 4. continued (R/t = 2.0, h/t = 0.5; F = K/(S$(\pi a/Q)^{1/2}$))

ϕ_3 (degrees)	F a/c = 2.0		
	a/t = 0.2	a/t = 0.3	a/t = 0.4
0	2.2916	2.3177	2.3485
19.425	2.2901	2.3214	2.3334
36.052	2.2611	2.3039	2.3085
49.107	2.2015	2.259	2.2686
59.21	2.1159	2.1867	2.2102
67.239	2.0105	2.0906	2.1314
73.898	1.8698	1.9796	2.0352
79.686	1.7813	1.8711	1.9348
84.962	1.6973	1.7888	1.8592
90	1.6729	1.7688	1.8419

15
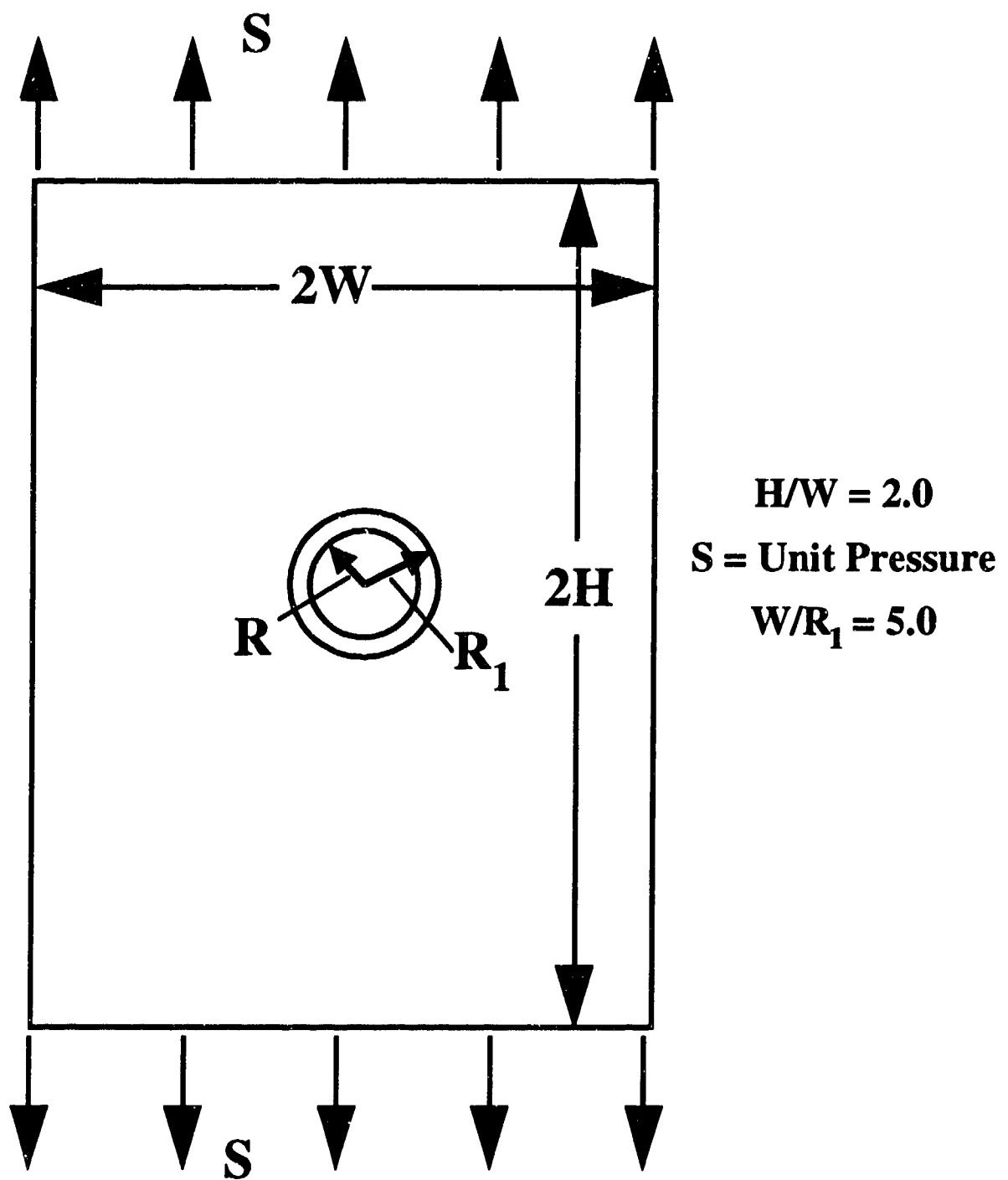
Figure 1. Specimen configuration and loading
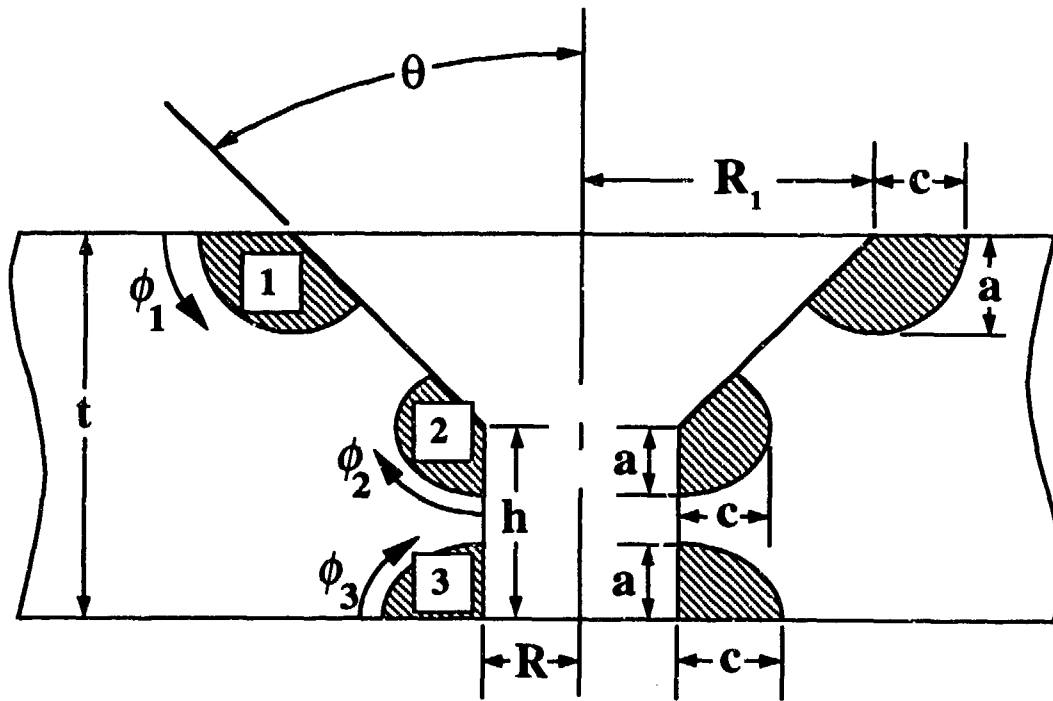
Figure 2.   Crack shapes and locations for countersunk hole; R/t = 2.0; h/t = 0.5; θ = 50°; a/c = 0.4, 0.7, and 2.0; a/t = 0.2, 0.3 and 0.4
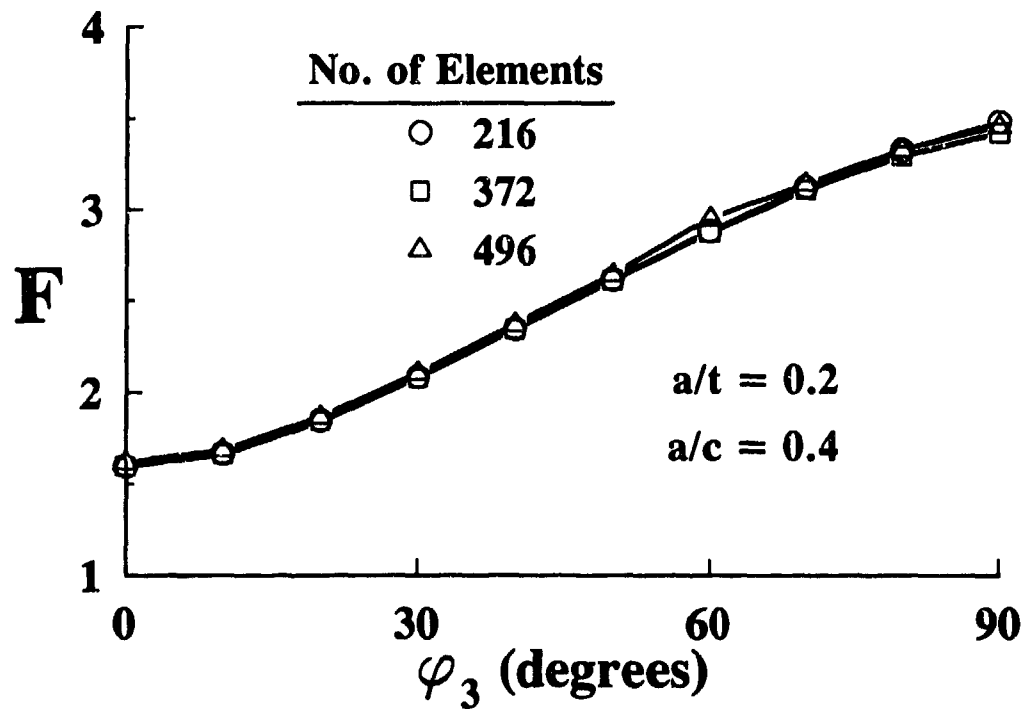
Figure 3.   Typical convergence study results, crack location 3, a/t = 0.2 and a/c = 0.4
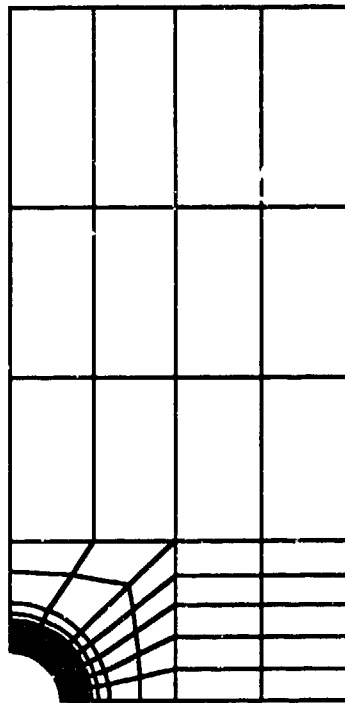
Figure 4(a).   Plan view of a typical finite-element mesh, 496 elements and 2655 nodes
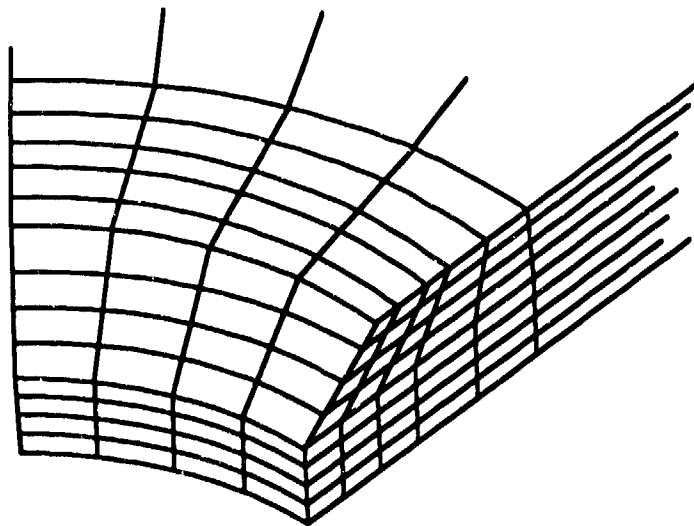
Figure 4(b).   Detailed view of finite-element mesh at crack location

18
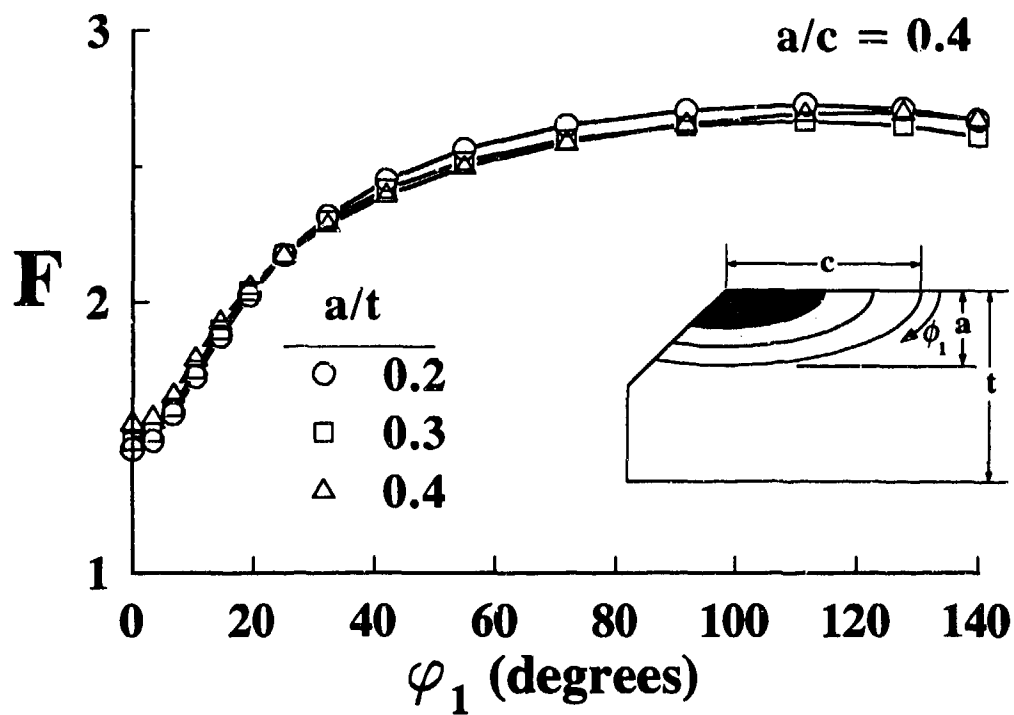
Figure 5.   Boundary correction factors F for crack location 1; a/c = 0.4
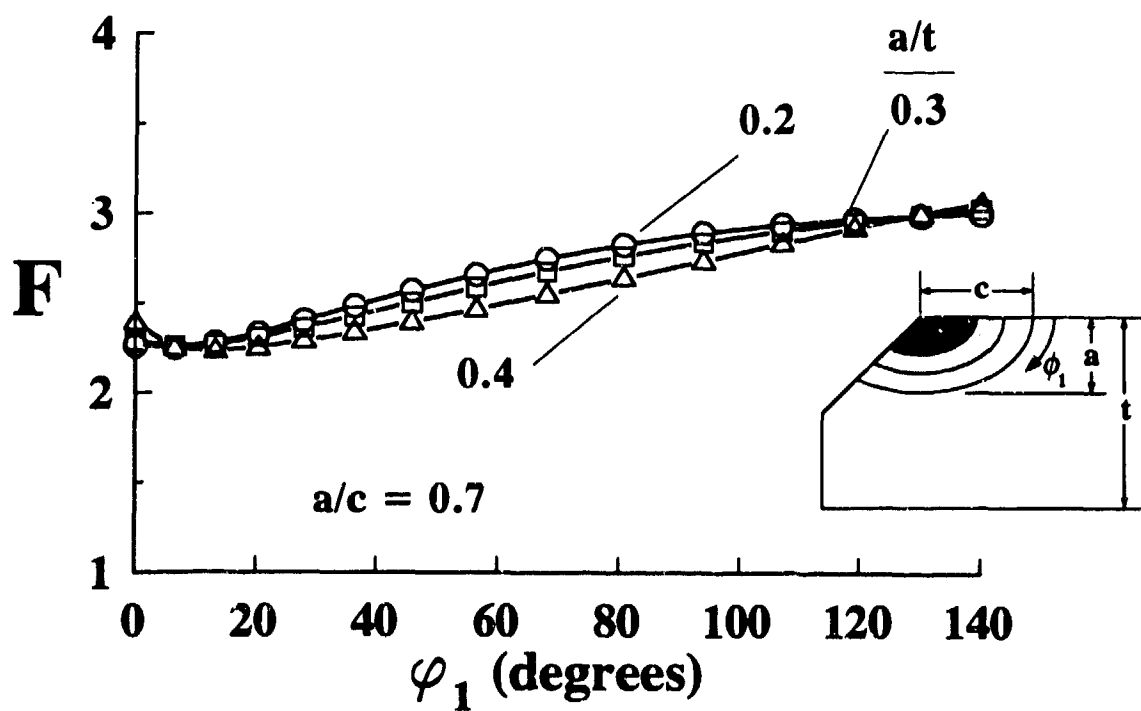
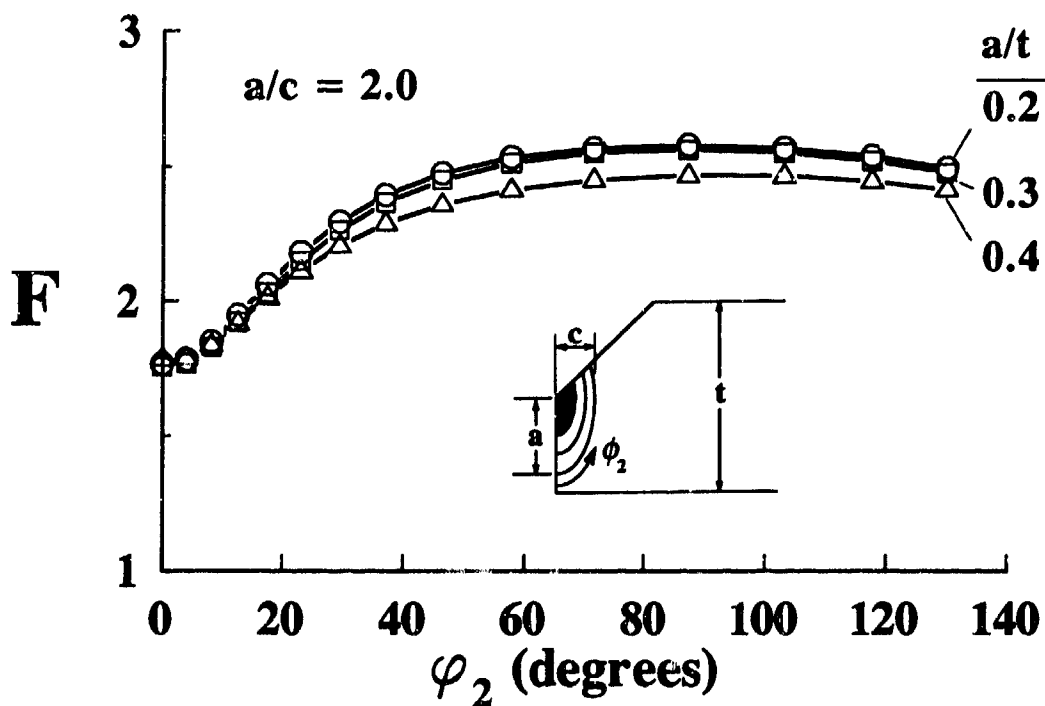Figure 6.   Boundary correction factors F for crack location 1; a/c = 0.7

19
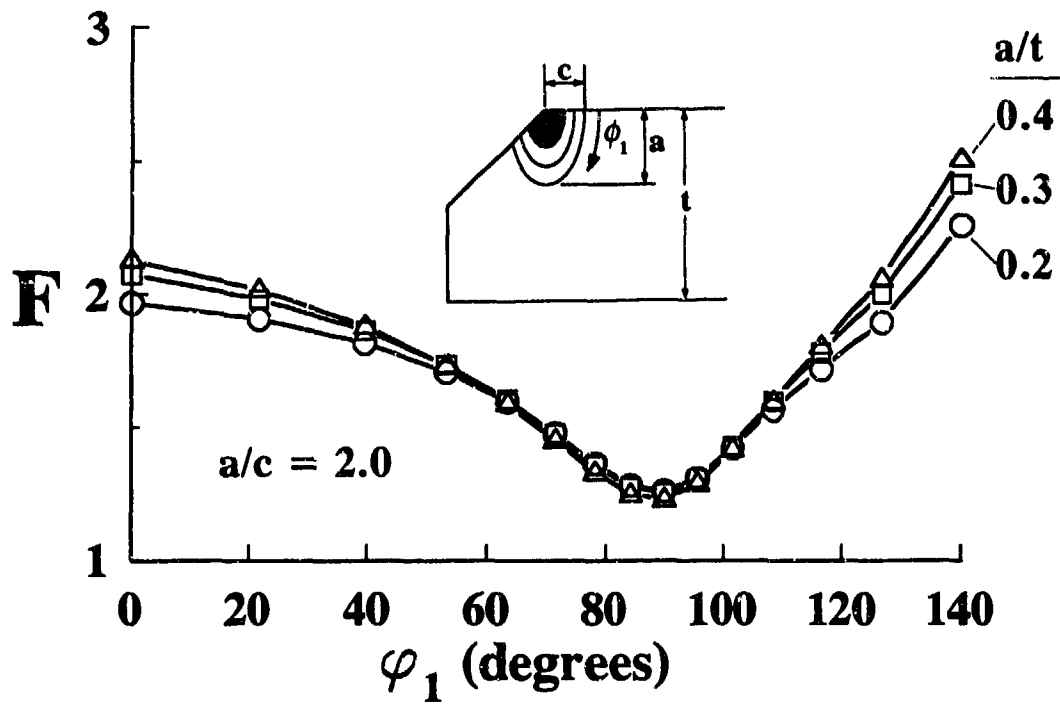
Figure 7.   Boundary correction factors F for crack location 1; a/c = 2.0
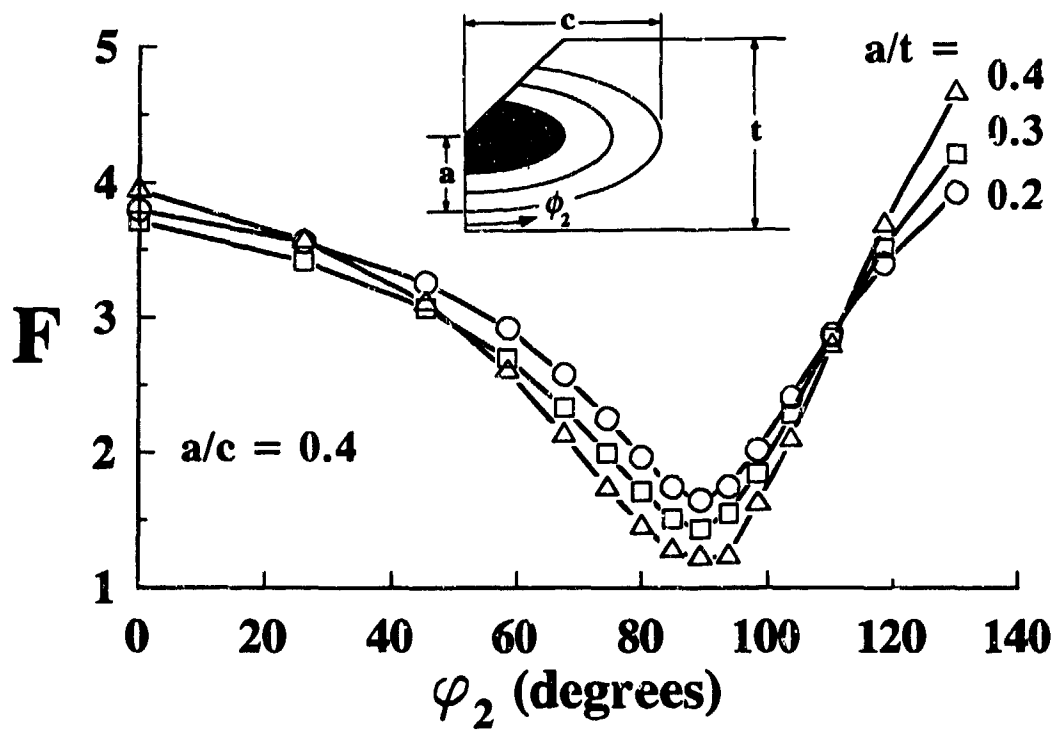
Figure 8.   Boundary correction factors F for crack location 2; a/c = 0.4
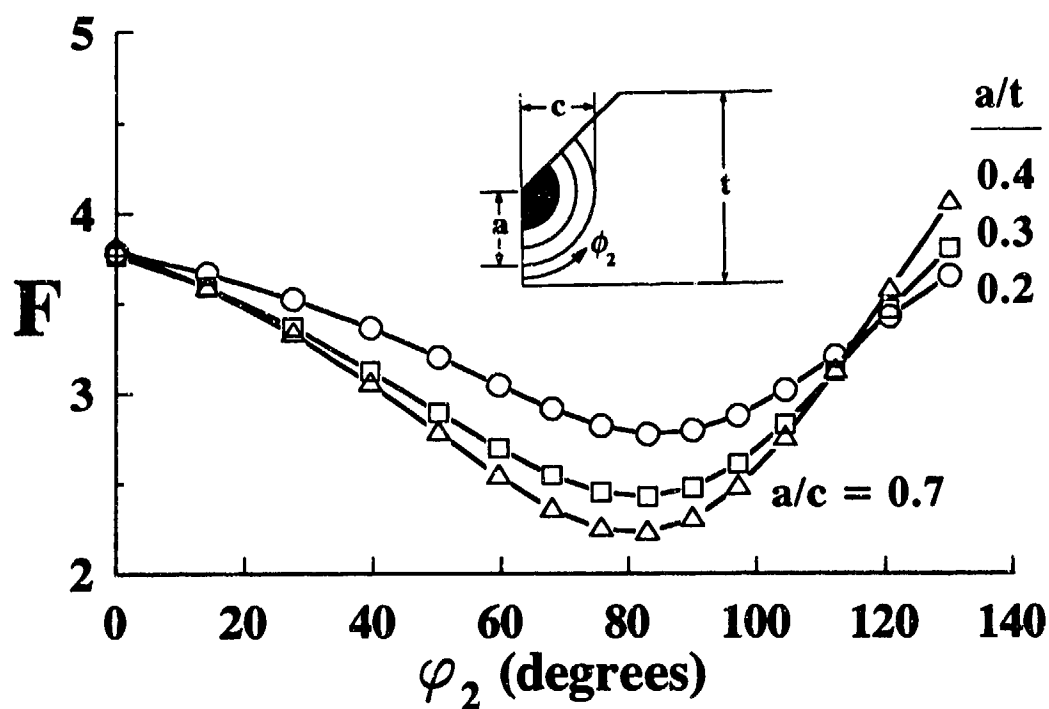
Figure 9.   Boundary correction factors F for crack location 2; a/c = 0.7

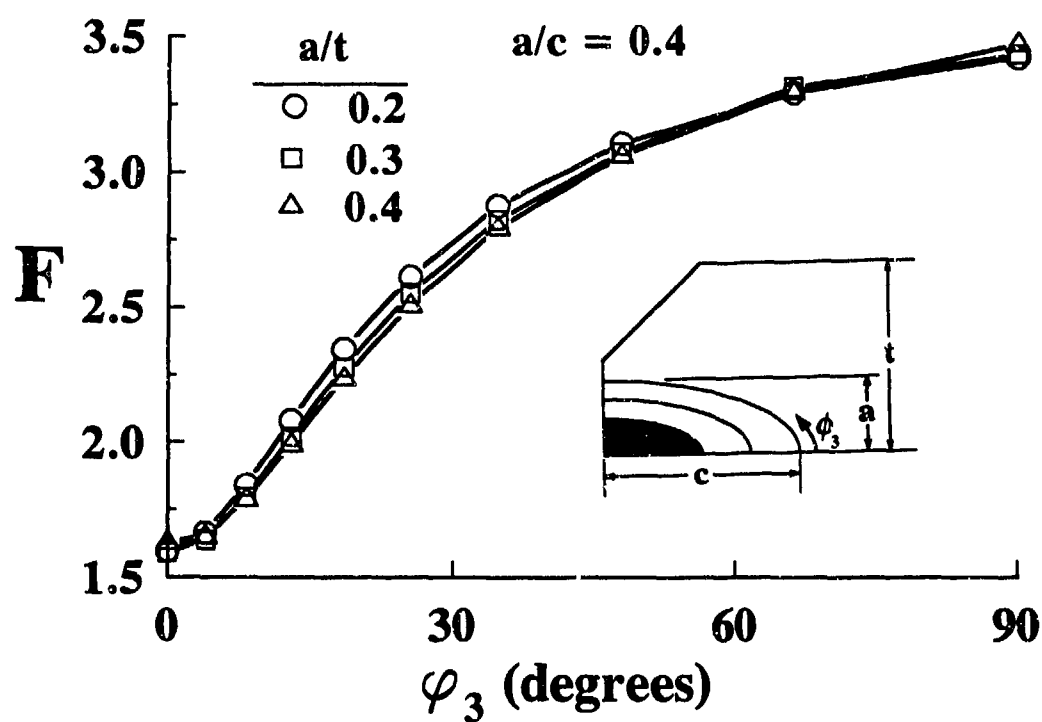Figure 10.   Boundary correction factors F for crack location 2; a/c = 2.0

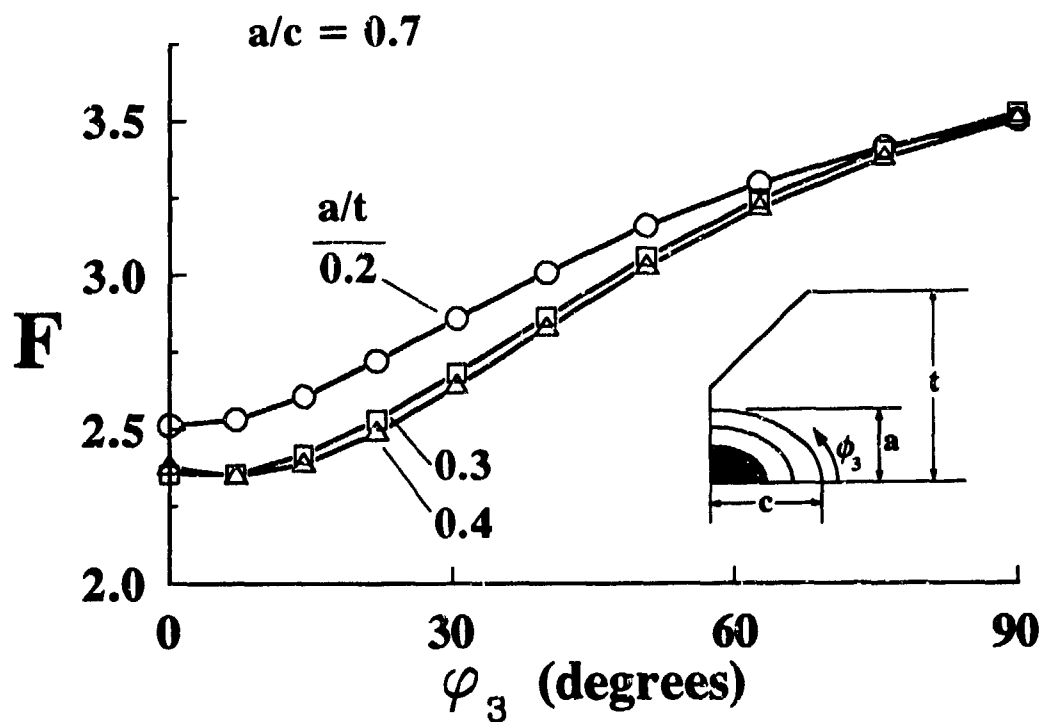Figure 11.   Boundary correction factors F for crack location 3; a/c = 0.4

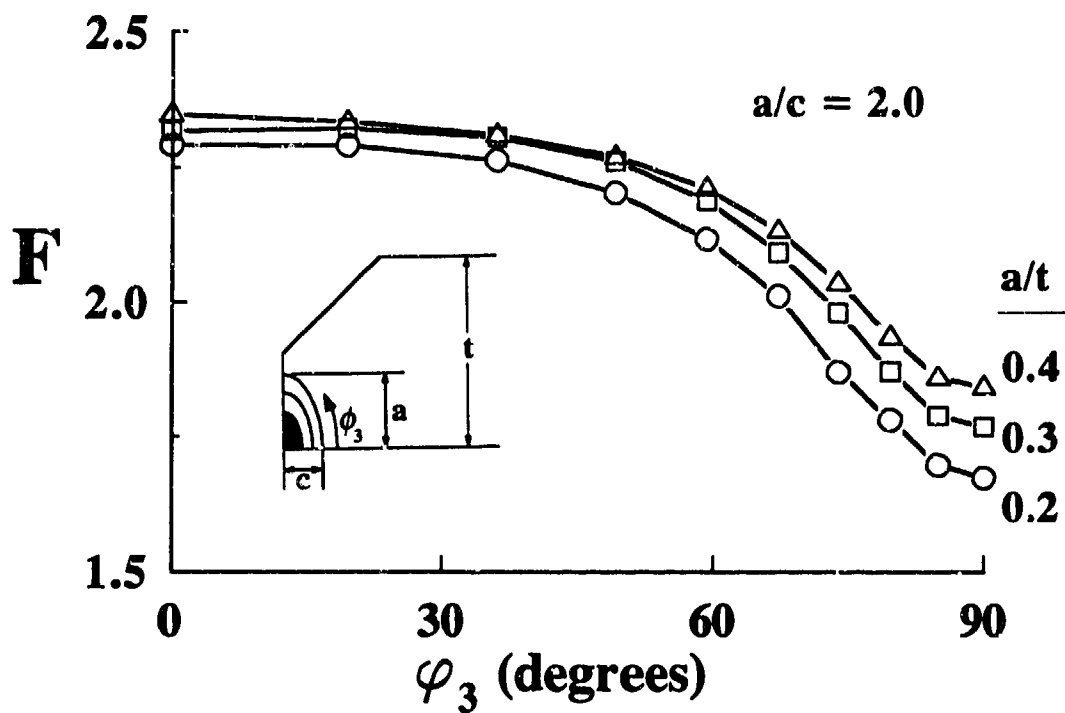Figure 12.   Boundary correction factors F for crack location 3; a/c = 0.7

22

Figure 13.   Boundary correction factors F for crack location 3; a/c = 2.0